

Reversible switching performance of water droplet-driven triboelectric nanogenerators using a magnetocontrollable lubricant-infused surface for sustainable power generation



Soyeon Yun^a, Suhyeon Cho^b, Hyeyon Woo Kim^{c,d}, Sung Beom Cho^{c,e}, Seunghyup Lee^{b,*}, Kijung Yong^{a,*}

^a Department of Chemical Engineering, Pohang University of Science and Technology, Pohang 37673, Republic of Korea

^b Nano-Convergence Materials Center, Korea Institute of Ceramic Engineering and Technology, Jinju 52851, Republic of Korea

^c Center of Materials Digitalization, Korea Institute of Ceramic Engineering and Technology (KICET), Jinju-si 52851, Republic of Korea

^d Division of Materials Science and Engineering, Hanyang University, Seoul 04763, Republic of Korea

^e Department of Materials Science and Engineering, Ajou University, Suwon 16499, Republic of Korea

ARTICLE INFO

Keywords:

Triboelectric nanogenerator
Reversible switching
Magnetocontrollable lubricant-infused surface
Self-powered sensor

ABSTRACT

Triboelectric nanogenerators (TENGs) are attracting great attention as potential renewable power sources; in particular, water droplet-driven liquid-solid (LS) TENGs are highly useful due to their abundant sources in daily life. This study developed a novel approach for switching the LS triboelectrification by using a magneto-controllable lubricant-infused surface (MCLIS). The basic units of the MCLIS-based TENG (MCLIS-TENG), that is, magnetocontrollable microwires, showed different alignment states, i.e., vertically standing or lying down, depending on the direction of the applied magnetic field. These reversible wetting states generated distinctive voltage outputs of ~2 V (ON state) and < 0.5 V (OFF state), correspondingly. ON/OFF cycles revealed excellent reversibility and stability even after 90 cycles. The switching characteristics of the MCLIS-TENG were studied systematically by varying the Weber number, inclination angle, and lubricant thickness. The proposed device also demonstrated highly sustainable power generation by utilizing the switchable wetting states even under high humidity, where the performance of most LS-TENGs degraded due to surface wetting problems. In addition, the MCLIS-TENG based self-powered magnetic proximity sensor is proposed as an exemplary application to detect the magnetic field intensity and the location of sensing object. This work provides a new idea of magneto-responsive triboelectric switching, widening the TENG usability in low-power-consumption applications such as wireless switches and self-powered sensors.

1. Introduction

Triboelectric nanogenerators (TENGs) have attracted increasing attention as renewable power sources that convert mechanical energy into electrical energy. Their working mechanism is based on the combination of triboelectrification and electrostatic induction. When two materials with diverse triboelectric polarities are contacted, electron or ion transfer induces a potential difference on their contact surfaces; as the cycle of contact and separation is repeated, electrons flow through an external load, generating a continuous electrical output. Various TENGs based on solid–solid triboelectrification have been explored due to their easy fabrication and low cost, as well as the wide range of

available materials [1–8].

Another type of TENGs, based on liquid–solid (LS) triboelectrification, is drawing attention since Wang group first reported a prototype [9]. In particular, water droplet-driven TENGs are highly useful because water energy sources exist abundantly everywhere in the forms of river/ocean waves and raindrops [10–13]. The electric double layer (EDL) theory explains LS triboelectrification, where electron transfer is key [14]. Most previous studies focused on increasing the amount of electrical output from the perspective of power generation. In general, TENG has a high inner impedance which leads to low current output [15]. Various attempts have been made to enhance and optimize the power generation, such as the introduction of micro/nano

* Corresponding authors.

E-mail addresses: shbelly@kicet.re.kr (S. Lee), kyong@postech.ac.kr (K. Yong).

hierarchical structures [16], surface functionalization [17,18], the pre-injection of electrical charges [19,20], and the development of various materials and electrode structures [21]. Despite all these efforts, the generated power is still too low to use LS-TENGs as efficient power sources.

To extend the applicability of TENGs, intelligent approaches are required in low power consumption. An example is achieving reversible switching controllability of the electrical output by external stimuli, which has wide potential applications in self-powered sensors and switches [22–27]. When LS-TENGs have switchable LS interfacial states such as wettability driven by various external stimuli, they can generate reversible switching power. However, despite the necessity of this triboelectric switching ability, few studies have been conducted on the reversible switching of LS triboelectrification. As a rare example, a temperature-sensitive LS-TENG could reversibly regulate triboelectrification by thermal stimuli [28]. The reversible switching of the electrical output was enabled by utilizing polycaprolactone (PCL) as a thermosensitive tribomaterial; the interfacial wettability of PCL is reversibly changed according to its temperature, which induces a change in the surface structure and, consequently, the LS triboelectrification switching. The interfacial wettability and surface

structure can be modulated also by other external stimuli, including stress [29], electric fields [30], and magnetic fields [31]. Among them, switching by magnetic fields has the advantage of fast, easy, and highly reversible responses. Yong group recently demonstrated that a magnetocontrollable lubricant-infused surface (MCLIS) has a switching capability between slippery and sticky wetting states depending on the applied magnetic field direction, which is also applicable to reversible LS triboelectrification switching [32].

The present study proposes a novel approach for the magnetocontrollable switching of LS triboelectrification by using an MCLIS as a triboelectric layer. The MCLIS was fabricated by aligning an array of magnetocontrollable microwires (MCMws) on a flat polydimethylsiloxane (PDMS) layer to provide triboelectric charges; the MCMws consisted of cobalt and PDMS, and they were coated with superhydrophobic nanoparticles. The MCLIS layer was completed by infiltrating fluorinated oil on this hierarchical structure, where the MCMws stood vertically or laid down (corresponding to the ON or OFF states, respectively) reversibly according to the direction of the applied magnetic field. When water droplets contacted the ON or OFF state surfaces, the MCLIS-based TENG (MCLIS-TENG) generated a voltage output of, respectively, ~2 V (ON state) or < 0.5 V (OFF state). It is

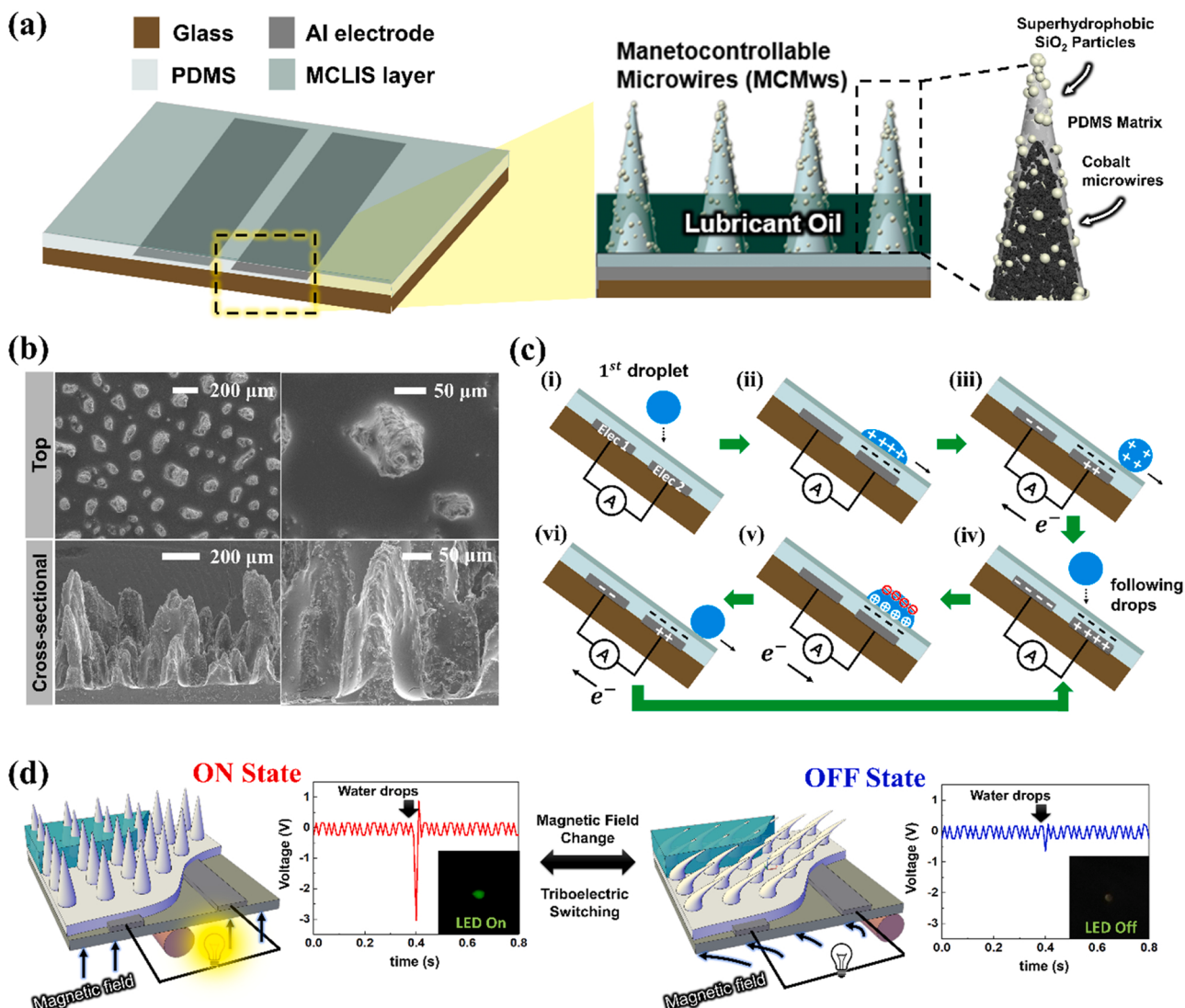


Fig. 1. Triboelectric nanogenerator based on a magnetocontrollable lubricant-infused surface. (a) Device structure. (b) Top and cross-sectional scanning electronic micrographs of the cobalt-infused polydimethylsiloxane (PDMS) microwires on its surface. (c) Working mechanism of the LS triboelectrification device. (d) Triboelectric switching from vertically standing (ON state) to lying down (OFF state) by changing the direction of the applied magnetic field. In the inset, the LED connected to the MCLIS-TENG is turned on or off in the different switching states.

known that liquid-liquid triboelectrification has a much weaker charge transfer than liquid-solid triboelectrification [14]. Therefore, this switching behavior could be explained by the formation and destruction of a continuous lubricant layer on the MCMws, which strongly affects the number of charges induced by triboelectrification between the water droplets and MCMws. Our MCLIS-TENG showed high durability and reversibility in repeated cycles, with a stable switching electrical output; its switching characteristics were studied systematically by varying the Weber number, inclination angle, and lubricant thickness. Moreover, the MCLIS-TENG attained highly sustainable power generation by utilizing these switchable wetting states even under high humidity, where the performance of most LS-TENGs degrade due to surface wetting problems. In addition, the MCLIS-TENG device has been proposed as a self-powered sensor to detect the magnetic proximity.

2. Results and discussion

Fig. 1a illustrates the basic structure of the MCLIS-TENG, which consisted of a glass substrate, aluminum electrodes, an MCLIS film on a flat PDMS layer acting as a solid friction layer, and lubricant oil. The Al electrodes were deposited on the glass substrate in the freestanding mode. The basic units of the MCLIS film were the MCMws; they were built via a simple template-free method by using a mixture of PDMS and ferromagnetic cobalt particles. PDMS is the one of the commonly used negative triboelectric materials due to its high electronegativity, mechanical strength and flexibility [33]. The application of a magnetic field in a vertical direction to the substrate resulted in a vertically aligned array of MCMws, whose diameter, height, and density were modulated according to the cobalt weight percentage in the PDMS solution. The optimum weight ratio between PDMS elastomer, curing agent, and cobalt particles was 1:1:2 (in wt%), as confirmed by comparing the MCMws dimension and electrical output (**Figs. S1 and S2**, Supporting Information). According to a scanning electron microscopy analysis (**Fig. 1b**), the average height and diameter of the MCMws were ~ 580 and $\sim 170 \mu\text{m}$, respectively. The X-ray diffraction (XRD) pattern of the MCMws in **Fig. S3** (Supporting information) showed the cobalt metal peaks. The cobalt particles have a uniform distribution in the MCMws as shown in **Fig. S4** (Supporting Information) with EDS elemental mapping. Hydrophobic SiO_2 nanoparticles were spray-coated on the MCMws to enhance their hydrophobicity; on this hierarchical solid friction layer, a lubricant with low surface energy (Krytox) was infiltrated to complete the MCLIS layer. The type of infusing lubricant can be an important factor for achieving optimal performance because the coverage over the porous structure can be varied depending on the type of lubricant [34]. The MCLIS-TENG was fabricated with different type of lubricant and the Krytox infiltrated samples showed the most stable performance (**Fig. S5**, Supporting Information).

The functioning of the fabricated MCLIS-TENG can be described as the well-known mechanism of freestanding-mode TENGs as follows (**Fig. 1c**) [35]. When the first water drop contacts the MCLIS layer in **Fig. 1c(ii)**, due to the contact electrification between the water drop and the MCLIS, the MCLIS gets negative charges while the water drop gets positive charges [36]. When the water drop shrinks and slides down, to reach the electrostatic equilibrium state with negative induced charges on the surface above electrode 2, electrons move from electrode 2 to electrode 1 in **Fig. 1c(iii)**. MCLIS layer can retain and be saturated with negative charges as a result of contact electrification after continuous droplet impinging [21]. When following water drop contacts and spreads on the MCLIS layer, it forms an electric double layer with MCLIS partly screening the negative charges on MCLIS and establishes electric potential difference [9]. Then, the electrons flow from electrode 1 to electrode 2 as shown in **Fig. 1c(v)** to reach a new equilibrium. When the water drop shrinks and leaves the MCLIS layer, screened negative charges on MCLIS layer are recovered and the electron flow occurs in opposite direction to achieve another new equilibrium (**Fig. 1c, vi**). Following water droplets can generate electrical output continuously by

the cycle of contact and separation (**Fig. 1c, iv-vi**). Electrical potential generation during the cycle through finite element method (FEM) simulation is conducted using AC/DC module in COMSOL software. The simulated potential difference result shows consistency with the working mechanism (**Fig. S6**, Supporting Information).

Fig. 1d displays the switching behavior of the LS triboelectrification, that the transferred charges can be changed with the external stimuli. By controlling the direction of magnetic field applied to the device, the structural state of MCMws can be changed and eventually triboelectrification characteristics can be switched. When the magnetic field is applied in vertical direction to the MCLIS, the MCMws align vertically. Then, those protruding through the lubricant layer make large triboelectric contact area with the water droplet, generating a large voltage output; this state is called the ON state. When the magnetic field direction deviates from the vertical direction, the MCMws lie down in that direction and are covered by the lubricant layer. Under this circumstance, the voltage output decreases significantly due to the triboelectrification interference by the lubricant layer; this state is called the OFF state. This structural change of the MCMws is completely reversible thus the electrical switching is reversible, as well. The triboelectric switching of MCLIS-TENG was further confirmed through a light-emitting diode (LED) connected to the device being turned on and off according to the change of the MCMws states.

The switchable triboelectric property of our MCLIS-TENG is closely related to the convertible wetting states of MCLIS. As shown in **Fig. 2a**, in the ON state (i.e., vertically aligned MCMws), the measured water contact angle (WCA) was $154.8 \pm 0.1^\circ$, sliding angle (SA) was 22° and contact angle hysteresis (CAH) was 28.72° (**Fig. S7**, Supporting Information), indicating a slippery Wenzel state [37] due to the MCMws protrusion through the lubricant layer. The slippery Wenzel state is a case where the water drop exists as the Wenzel state on the surface where lubricant is infused into the hierarchical structure, but sliding is possible at an angle that is not large. In the OFF state (lying down MCMws), the WCA decreased to $118.5 \pm 0.1^\circ$, SA was 8° and CAH was 3.0° , showing a sliding behavior of water droplets like that on slippery lubricant-infused porous surfaces (SLIPS); in this slippery state, the droplet directly contacts a nearly continuous lubricant layer covering the MCMws. This convertible wetting characteristics are originated from the ferromagnetic cobalt particles inside the elastic PDMS matrix, as presented in our previous study [32]. The **Fig. 2a** shows that the structure of MCMws is changed as the magnetic bar is moved which means the direction of magnetic field is changed. **Fig. 2b, c** illustrates the triboelectric switching behavior of the MCLIS-TENG driven by a magnetic field in terms of open-circuit voltage (V_{OC}) and a short-circuit current (I_{SC}). Both V_{OC} and I_{SC} noticeably differed between the ON and OFF states at a given water drop height and inclination angle. In the ON state, the generated V_{OC} and I_{SC} were $1.35 \pm 0.12 \text{ V}$ and $2.03 \pm 0.24 \mu\text{A}$, respectively; in the OFF state, they dramatically decreased to $0.52 \pm 0.07 \text{ V}$ and $0.69 \pm 0.13 \mu\text{A}$. The generated electrical output ratio shows more than three in ON/OFF states, confirming a triboelectric switching driven by the reversible surface wetting states of MCLIS. In addition, the output power was measured by connecting different values of load resistances with each state. The maximum power for a single $50 \mu\text{l}$ water drop is $1.82 \mu\text{W}$ at $1.5 \text{ M}\Omega$ in ON state and $0.31 \mu\text{W}$ at $1.5 \text{ M}\Omega$ in OFF state. (**Fig. S8**, Supporting Information) The output power of MCLIS-TENG is comparable to the recently reported freestanding water drop TENG [27,38–40]. As we know, the output power reaches maximum value when the external resistance equals the internal impedance [13,41]. This suggests that our MCLIS-TENG works most effectively around a load of $1.5 \text{ M}\Omega$.

The underlying mechanism of this triboelectric switching was studied by investigating the role of the lubricant layer in both the ON and OFF states. The lubricant layer thickness (h_l) was controlled from 0 to $400 \mu\text{m}$ and the corresponding voltage output was measured in both states. In the ON state, the voltage reduction was negligible from 0 to $100 \mu\text{m}$, but the voltage output decreased gradually at higher h_l , and

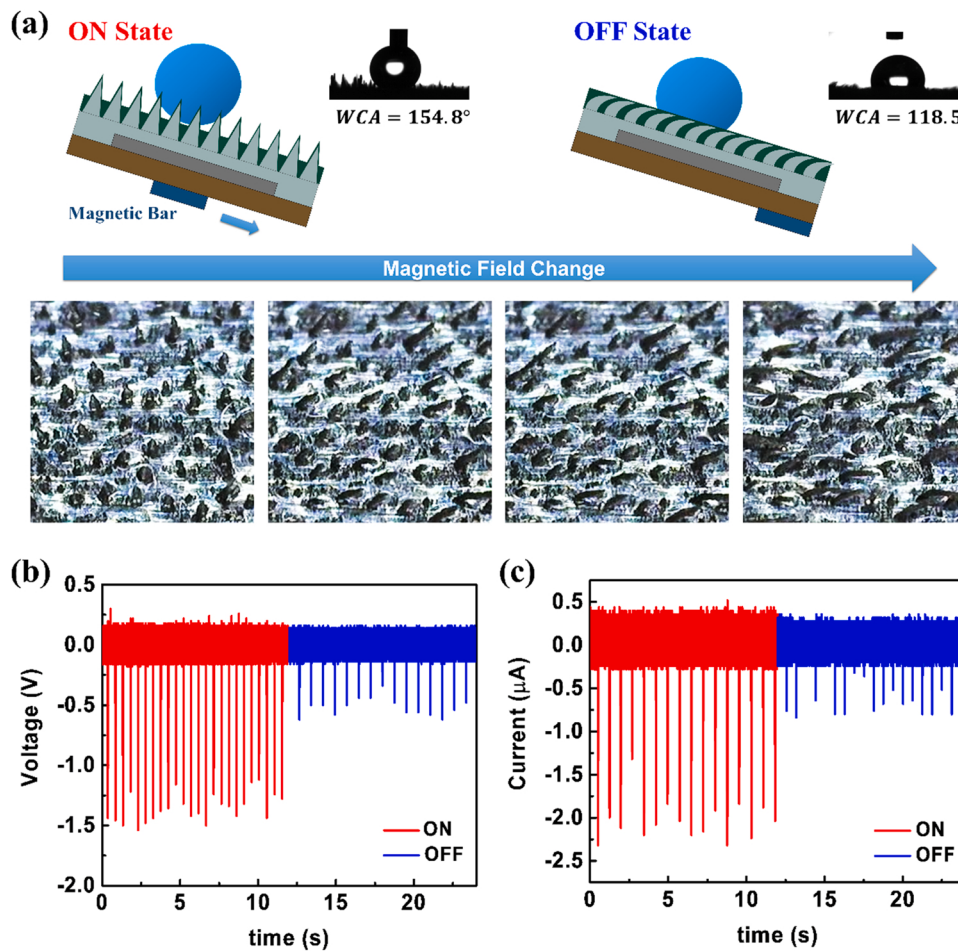


Fig. 2. Characteristics of the triboelectric nanogenerator based on a magnetocontrollable lubricant-infused surface (MCLIS). (a) Apparent characteristics of the ON (slippery Wenzel) and OFF (slippery) states of the MCLIS: the corresponding water contact angle (up) and the alignment shifting of the magnetocontrollable microwires with the magnetic field change (down). (b) Switching open-circuit voltage and (c) short-circuit current of the device at a fixed drop height and inclination angle of 5 cm and 45°, respectively.

almost no voltage was generated at 400 μm (Fig. 3a). In contrast, the voltage output more significantly changed in the OFF state (Fig. 3b); the voltage output drastically decreased at just $\sim 50 \mu\text{m}$ and showed further reduction at higher h_l . Fig. 3c summarizes these results for both states in terms of the voltage output dependence on h_l . With increasing h_l , the voltage output in the ON state decreased monotonically, while it dropped fast in the OFF state. The voltage generation, interestingly, differed only a little between the two states when no lubricant was added to the MCMws ($h_l = 0 \mu\text{m}$). These results confirm that the lubricant layer plays a critical role in the MCLIS-TENG by hindering direct triboelectrification between MCMws and water droplets. As illustrated in Fig. 3d, in the ON state, since the MCMws stand upright, protruding through the lubricant layer, a significant portion of them is exposed to direct contact with water droplets; the resulting direct contact electrification generates a high density of induced charges on the MCLIS-TENG. In the OFF state, where the MCMws lie down and can be fully covered with a continuous lubricant layer even at low h_l (Video S1, Supporting Information), the induced charge density is highly reduced by the screening effect of the lubricant in the direct contact electrification.

Supplementary material related to this article can be found online at doi:10.1016/j.nanoen.2022.107783.

The reversibility and stability of the electrical output are important factors for the switching characteristics of an MCLIS-TENG to be reliable and attractive in future applications. Therefore, the durability of our MCLIS-TENG switching voltage cycles was tested with a cyclic change of the MCMws alignment by periodically changing the magnetic field direction. In this experiment, the water droplets were dropped at a fixed height of 5 cm and an inclination angle of 45°. Fig. 4a shows a highly durable ON/OFF voltage output with a ratio of more than three several

cycles. Even after 90 cycles, the electrical output exhibited excellent switching stability (Fig. 4b) due to the durability of the MCMws as shown in SEM images which shows the state before and after cycling (Fig. S9, Supporting Information).

The switching characteristics of MCLIS-TENGs can be controlled by various parameters affecting the impact dynamics of the water droplets. In this regard, we studied the effects of the water drop height (h_d) and device inclination angle. Fig. 4c illustrates the h_d effect on the switching performance at an inclination angle of 45° for 50- μl -sized water droplets. The corresponding Weber number (We) is also reported; it was calculated as $We = \rho v^2 D / \sigma = \frac{2\pi g D}{\sigma} h_d$, where ρ is the water density, v and D are the droplet velocity and diameter, respectively, and σ is the surface tension of water. Except for v , all these parameters are intrinsic properties of water, thus, the We is directly proportional to the h_d . In both the ON and OFF states, the impact energy of the water droplets increased along with the We increase which means the converted electrical energy also increased, thus, the switching signal similarly rose as shown in Fig. 4c. The impact energy is directly related with the impact dynamics of water droplet, especially with the contact area and the speed. For the purpose of higher charge difference, i.e. higher voltage generation between the electrodes, a faster contact between the droplet and the surface would be advantageous. When a droplet in contact with the surface is spreading, the change of contact area between the droplet and electrode breaks the electrostatic balance, leading electrons to migrate from another electrode to overlapped electrode. Thus, the generated electrical outputs are proportional to the contact area change rate [42]. In other words, when the effective contact area that is defined as the maximum spreading area of the water droplet increased, the voltage output also rose because the number of triboelectrification-induced charges was

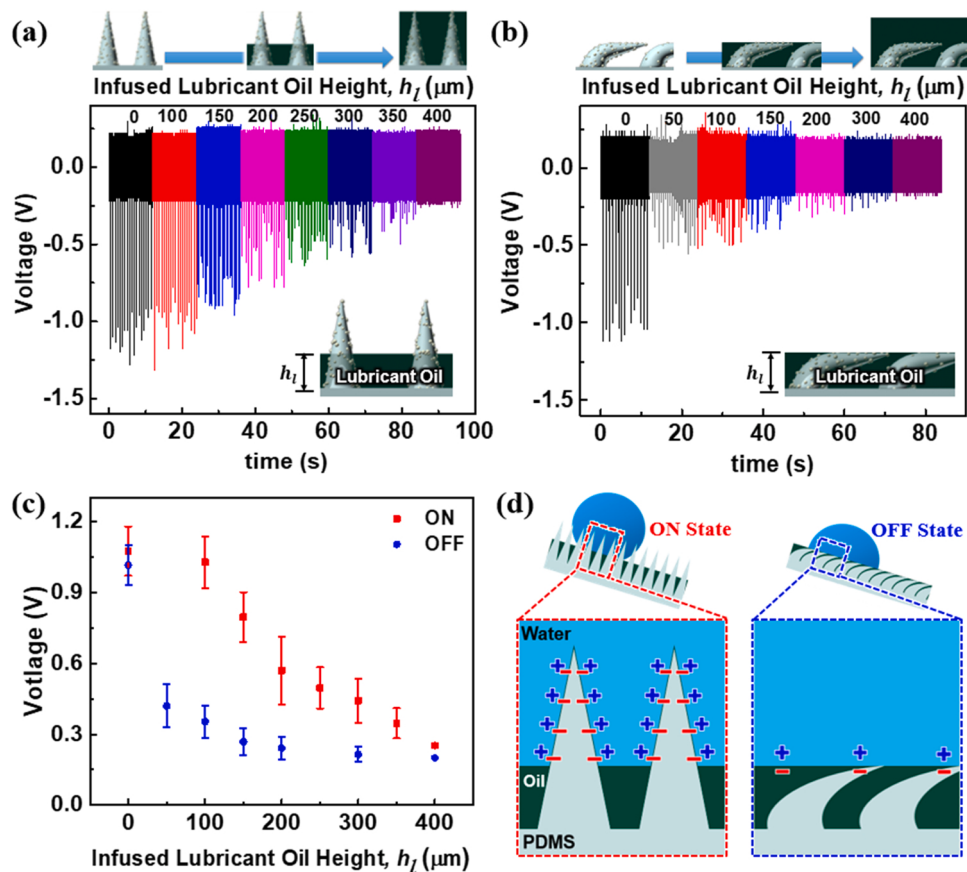


Fig. 3. Switching mechanism of the triboelectric nanogenerator based on a magnetocontrollable lubricant-infused surface (MCLIS). (a,b) Dependence of the electrical output on the lubricant layer thickness (h_l) when the magnetocontrollable microwires stand up (a) and lie down (b). (c) Relationship between h_l and voltage output in the ON and OFF states; h_l was calculated based on the volume of applied lubricant and the MCLIS area. (d) Triboelectric switching mechanism of the ON/OFF states.

proportional to the contact area. Thus, it would be obvious that with the higher We of droplet, the higher voltage, that is, the higher signal can be generated in this triboelectric based switching device. However, it should be noted that increasing the We of droplet over 60, the output voltage is saturated because of the fragmentation of droplet at the very moment of contact. At an h_d of 15 cm or higher, the too high impact pressure caused the droplets to be fragmented, resulting in a randomly distributed contact area, which eventually resulted in a fluctuated voltage output (Fig. S10, Supporting Information). Switching current output was also measured for various drop height and it shows consistent trend with voltage output. (Fig. S11, Supporting Information).

Another critical parameter affecting the impact dynamics is the inclination angle of the MCLIS-TENG with respect to the ground (Figs. S12 and S13, Supporting Information). Therefore, an inclination angle range of 20–70° was studied at a fixed h_d of 5 cm; 20° is the minimal angle to ensure that the droplets completely roll off the MCLIS. As shown in Fig. 4d, in the OFF state, the generated voltage change was negligible with the inclination angle; this suggests that the continuous lubricant layer maintains its OFF state characteristics with a low electrical output. In the ON state, instead, the generated voltage increased as the inclination angle reached 45°, but it decreased at higher angles. The inclination angle impact on the triboelectrification can be elucidated by the effect of the contact area change rate on the electrification charge density change, as well [42,43]. The contact area change rate (dS/dt) is considered for the time change from initial contact to detachment and the change value of contact area. Previous studies explained that dS/dt has a positive correlation and shows consistent tendency with electrical output. We measured dS/dt values by high-speed camera observations in top and side view as presented in Fig. 4e. As a result, the tendency was consistent to that of the voltage output for various inclination angle

conditions in ON state. The contact area change rate was the largest at 45°, leading to the generation of the highest voltage in the ON state. Unlike the We affecting overall impact dynamics parameters as discussed above, the contact area change rate can be selectively changed with controlling inclination angle. Through the optimization experiment on dynamics conditions, we could get information for the operating range capable of implementing stable switching characteristics of MCLIS-TENG and suggest the possibility for working as a sensor for dynamics condition. So far, the MCLIS-TENG was investigated as a potential switching device for the elucidation of its working mechanism and optimization of its characteristics. It should be noted that this switching device can be operated without external power source. As well as an energy harvester application, which is a traditional application of triboelectrics, such novel approach can be realized as wireless switches, and self-powered sensors.

The switchable wettability is a unique characteristic of our MCLIS-TENG, which has additional but important merit for sustainable power generation in various environments. Since LS-TENGs produce electrical power from the triboelectrification of water and the triboelectric layer, their performance inevitably degrades in a humid environment due to surface wetting problems. However, this performance degradation can be prevented in our MCLIS-TENG by its reversible switching wettability characteristics. To demonstrate this unique capability, the MCLIS-TENG was placed on a 5 °C cold plate in high humidity ambient condition. As shown in Fig. 5a, in the ON state, the high surface area of the MCMws allowed fast collection of water droplets from the fog; when the water droplets continued to gather and their volume was sufficiently large, the MCLIS was completely getting wet. The conversion into the wetting state greatly reduced the charges induced by LS triboelectrification, decreasing the electrical output (Fig. 5b and Fig. S14, Supporting

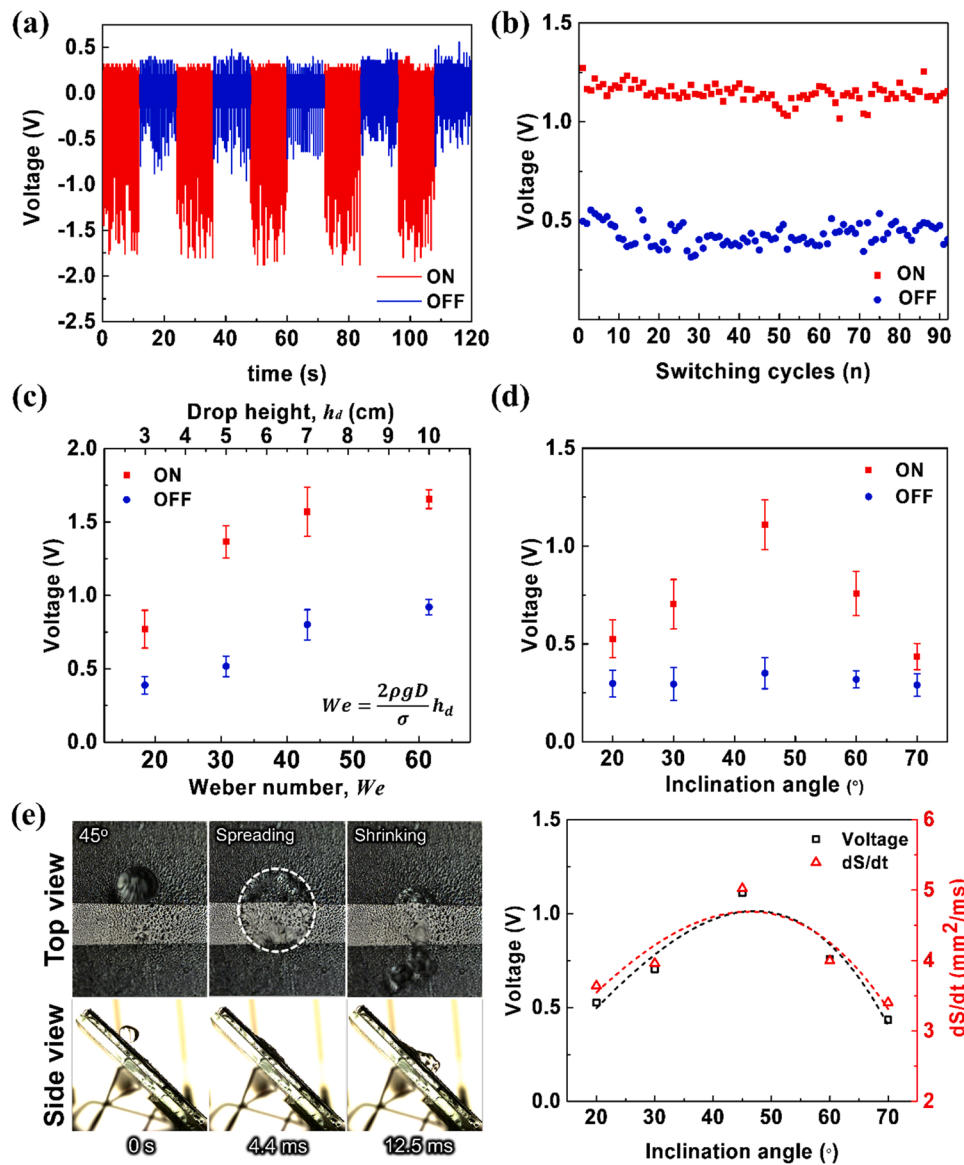


Fig. 4. Switching performance of the MCLIS-TENG. (a) Switching voltage cycles at a fixed drop height of 5 cm and an inclination angle of 45°. (b) Stability and reversibility assessed through switching cycles. (c) Switching behavior for various Weber numbers and corresponding drop heights. (d) Switching behavior for various inclination angles. (e) High-speed camera images of water droplet at contact, spreading, and shrinking moment with the MCLIS-TENG at 45° and the relationship between contact area change rate and voltage output.

Information). The condensate on the MCLIS-TENG surface could be removed by converting the ON state into the OFF one by changing the magnetic field direction. In the resulting slippery OFF state, the pinned droplets contacted the nearly flat lubricant layer, becoming unpinned and rolling off the surface. This phenomenon can be called cleaning because it removes the droplets covering the MCLIS and restores the screened triboelectrification (Fig. 5c). Triboelectrification recovery by cleaning was confirmed through the corresponding restoration of the voltage output (Fig. 5b). This result demonstrates the applicability of our MCLIS-TENG for sustainable power generation under highly humid and locally low temperature environment or sudden temperature change environment in which condensation of water vapor in the air can occur.

Taking advantage of the reversible magnetic field-dependent switching characteristics, as an exemplary application, the MCLIS-TENG was characterized as proof-of-concept self-powered magnetic proximity sensor. The magnetic proximity sensors detect the approach and position of the surrounding magnet or an object to which the magnet is attached [44,45]. These sensors use non-contact object detection beyond the normal limits of inductive sensors [46]. Fig. 6a shows a schematic diagram of the MCLIS-TENG system as a self-powered magnetic proximity sensor. There is a magnet attached to the sensing object and the MCLIS-TENG is fixed in position. Sensing distance (d) is

defined as the distance from MCLIS-TENG to the sensing object. In this case, the proximity information would be obtained through an electric signal generated according to the sensing distance.

We evaluated its performance at a fixed drop height 5 cm and inclination angle 45° with DI water and a 510 mT neodymium magnet (Fig. 6b-c). The magnetic field intensity at a point by a magnet is inversely proportional to the distance away from the magnet [47]. In the case of MCLIS-TENG, the stronger the magnetic field intensity, the more MCMws lie down and less triboelectrification occurs due to the interference by lubricant, resulting the reduction of the generated voltages. When the sensing distance is within 1 cm, the generated voltage is about 0.6 V, which shows the OFF state characteristics as shown in Fig. 6c. As the sensing distance increases, the generated voltage also increases to about 1.4 V. The MCMws also remain standing without lying down any longer for the magnetic field intensity below a certain level. Accordingly, the generated voltage is saturated at a certain distance or more, which indicates the aforementioned ON state characteristics (Fig. S15, Supporting Information), and the voltage at this time was defined as V_{max} . As the sensing distance varies depending on the strength of the magnetic system used for sensor, the generated voltage was also measured by changing the superficial magnetic field intensity of the magnet. In the case of 410 mT magnet, the generated voltage was

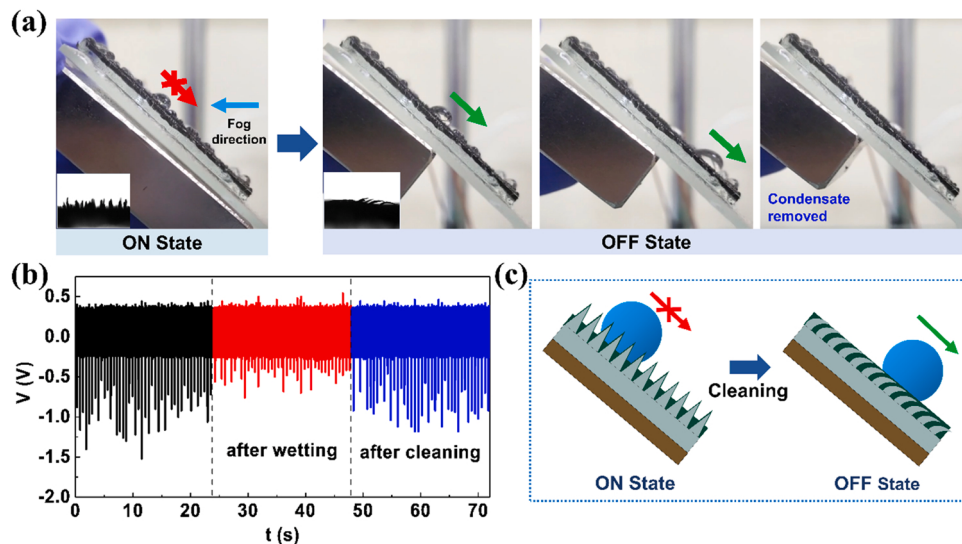


Fig. 5. Power output regeneration by cleaning of the MCLIS-TENG. (a) Cleaning performance for sustainable power generation in an extremely humid environment. (b) Cleaning effect on the restoration of the electrical output. (c) Cleaning process.

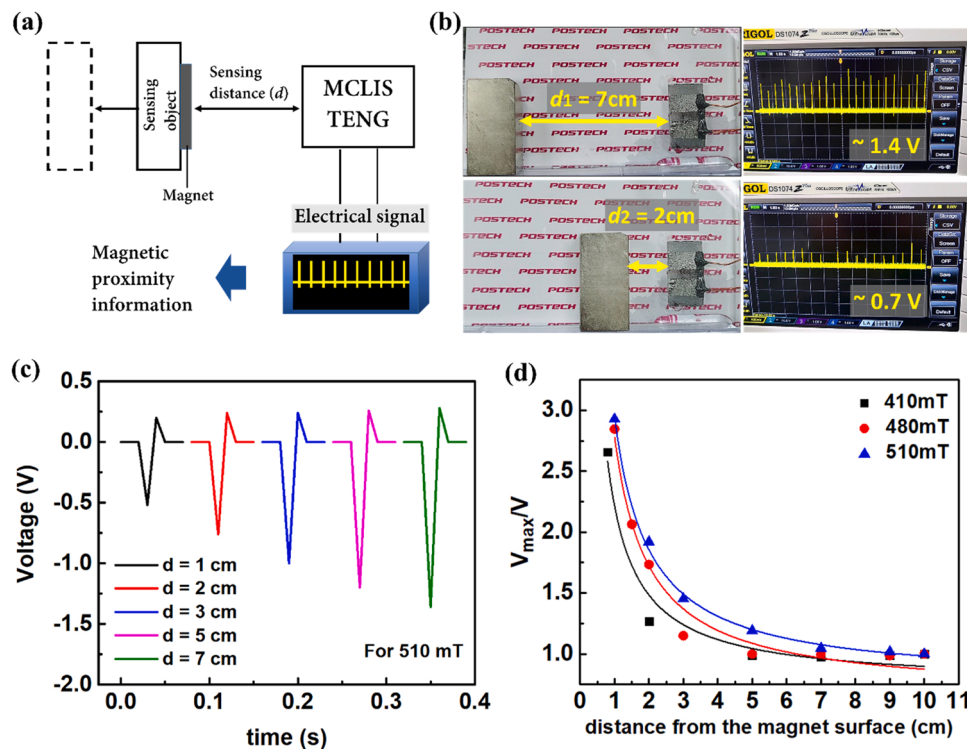


Fig. 6. The application of MCLIS-TENG as a magnetic proximity sensor. (a) A schematic diagram of the MCLIS-TENG based self-powered magnetic proximity sensor. (b) A digital image of the characterization process of MCLIS-TENG sensor with DI water and a 510 mT neodymium magnet. (c) The electric signal of MCLIS-TENG as the sensing distance changed with 510 mT magnet. (d) A fitting plot for V_{max}/V corresponding to the sensing distance.

reached to V_{max} at a distance of 5 cm, while 480 and 510 mT magnets were reached at a distance of 7 cm (Fig. S16, Supporting Information). To confirm the sensitivity of MCLIS-TENG as a magnetic proximity sensor, we defined new parameter V_{max}/V which is considered to be proportional to the magnetic field intensity at a point. V is the measured voltage value at a point. Fig. 6d is the inversely proportional fitting of the plot for V_{max}/V and sensing distance. The high R square value shows V_{max}/V is inversely proportional to sensing distance, which is consistent with the fact that the magnetic field intensity at one point is inversely proportional to the distance away from the magnet. The results

here demonstrate the feasibility of detecting not only the presence of a magnetic field, but also the exact location of an object as a self-powered magnetic proximity sensor. We present new ideas for research fields in self-powered and wireless sensors by applying a new type of TENG switched by a magnetic field.

3. Conclusion

We have presented an original concept of reversible triboelectric switching characteristics stimulated by a magnetic field change. When

the magnetic field direction changes over the MCLIS, its MCMws switch their alignment between the vertically standing and lying down states. Due to this phenomenon, the triboelectric power generation output of the proposed MCLIS-TENG differs nearly three times between these two states, which can be utilized as a triboelectric switching. The mechanism of triboelectric switching is explained by the lubricant layer interference in the LS triboelectrification. In the ON state, the protruded MCMws can directly contact the water droplets, securing sufficient LS triboelectrification. In the OFF state, however, the MCMws lying within the lubricant layer have an insufficient contact area with the water droplets, which lowers the triboelectric charge. After multiple cycles of structural switching by magnetic field variation, the electrical output still has reliable reversibility and stability because of the reversible MCMws alignment. The detailed triboelectric switching characteristics were investigated systematically depending on various impact dynamic parameters. The results also showed that the structural change of the MCLIS affects its wettability and, hence, the MCLIS-TENG possesses a cleaning function for sustainable power generation in humid environments, confirming its practical applicability. Additionally, the MCLIS-TENG is applied as a self-powered magnetic proximity sensor. This novel approach of triboelectric switching could have major effects on the research fields regarding energy harvesters, wireless switches, and self-powered sensors.

4. Experimental section

4.1. Materials

An Al tape, PDMS Base (Sylgard 184), a curing agent, and cobalt microparticles (average diameter of 2 μm , Sigma Aldrich) were used.

4.2. MCLIS preparation

The PDMS base, curing agent, and cobalt microparticles were mixed in a 1:1:2 wt ratio. After sufficient stirring, proceed by dividing into spin coating secondary steps. The first and second rounds were run for, respectively, 5 s at 500 rpm and 20 s at 2000 rpm. With a heat-resistant magnet (50 mm \times 50 mm \times 20 mm, superficial magnetic field intensity of 4500 Gs), a magnetic field was applied vertically to the substrate, with annealing at 95 °C for 1 h. Spray coating SiO₂ nanoparticles in an ethanol solution that was previously SAM-treated for superhydrophobicity; fluorinated oil (DuPont Krytox 103) was infused.

4.3. MCLIS-TENG fabrication

A cleaned glass was prepared as the substrate. A pair of Al tapes (1 cm \times 2 cm, with a 0.5 mm gap) was attached to the substrate in the freestanding mode. The stabilization layer (PDMS base:curing agent = 10:1) was doctor-bladed to obtain a thickness of 150 μm . Then, the MCLIS was fabricated on the stabilization layer.

4.4. Characterization

The static WCA was measured using a droplet analyzer (SmartDrop, Femtofab). High-resolution images of the MCMws structures were obtained by field emission scanning electron microscopy. The V_{OC} and I_{SC} were measured using, respectively, a digital oscilloscope (DS1074Z Plus, Rigol) and a low-noise current amplifier (SR570, Stanford Research System). The lubricant thickness was controlled by its infused volume (V) and MCLIS area (A) as $h = V/A$. The effective contact area of the water droplets was derived from top view high-speed camera images recorded at a frame rate of 3600 fps.

4.5. Cleaning experiment

The condition of system was measured by a thermo-hygrometer

(Thermo-Hygro MS 83, Dostmann). The humidifier was used to maintain for 85% RH condition with 25 °C ambient temperature and the measured MCLIS-TENG surface temperature was 5 °C on the cooling plate.

CRediT authorship contribution statement

Soyeon Yun, Seunghyup Lee, Kijung Yong: Conception and design of study. **Soyeon Yun, Suhyeon Cho, Seunghyup Lee:** Investigation and Data curation. **Soyeon Yun, Seunghyup Lee:** Writing – original draft preparation. **Soyeon Yun, Hyeon Woo Kim, Sung Beom Cho, Seunghyup Lee:** Writing – review & editing. **Seunghyup Lee, Kijung Yong:** Supervision. **Kijung Yong:** Funding acquisition.

Declaration of Competing Interest

The authors declare that they have no known competing financial interests or personal relationships that could have appeared to influence the work reported in this paper.

Data availability

Data will be made available on request.

Acknowledgments

This work was supported by the National Research Foundation of Korea (NRF) grant funded by the Korea government(MSIT) (NRF-2021R1A5A1084921, NRF-2021K1A4A8A02079226).

Appendix A. Supporting information

Supplementary data associated with this article can be found in the online version at doi:[10.1016/j.nanoen.2022.107783](https://doi.org/10.1016/j.nanoen.2022.107783).

References

- [1] S. Wang, L. Lin, Y. Xie, Q. Jing, S. Niu, Z.L. Wang, Sliding-triboelectric nanogenerators based on in-plane charge-separation mechanism, *Nano Lett.* 13 (2013) 2226–2233, <https://doi.org/10.1021/nl400738p>.
- [2] Y. Yang, H. Zhang, J. Chen, Q. Jing, Y.S. Zhou, X. Wen, Z.L. Wang, Single-electrode-based sliding triboelectric nanogenerator for self-powered displacement vector sensor system, *ACS Nano* 7 (2013) 7342–7351, <https://doi.org/10.1021/nn403021m>.
- [3] L. Lin, Y. Xie, S. Niu, S. Wang, P.K. Yang, Z.L. Wang, Robust triboelectric nanogenerator based on rolling electrification and electrostatic induction at an instantaneous energy conversion efficiency of ~55%, *ACS Nano* 9 (2015) 922–930, <https://doi.org/10.1021/nm506673x>.
- [4] G. Zhu, Z.H. Lin, Q. Jing, P. Bai, C. Pan, Y. Yang, Y. Zhou, Z.L. Wang, Toward large-scale energy harvesting by a nanoparticle-enhanced triboelectric nanogenerator, *Nano Lett.* 13 (2013) 847–853, <https://doi.org/10.1021/nl4001053>.
- [5] W. Seung, M.K. Gupta, K.Y. Lee, K. Shin, J. Lee, T.Y. Kim, S. Kim, J. Lin, J.H. Kim, S. Kim, Nanopatterned Textile-Based Wearable Triboelectric Nanogenerator, *ACS Nano* 9 (2015) 3501–3509.
- [6] K.Y. Lee, J. Chun, J.H. Lee, K.N. Kim, N.R. Kang, J.Y. Kim, M.H. Kim, K.S. Shin, M. K. Gupta, J.M. Baik, S.W. Kim, Hydrophobic sponge structure-based triboelectric nanogenerator, *Adv. Mater.* 26 (2014) 5037–5042, <https://doi.org/10.1002/adma.201401184>.
- [7] S. Kim, M.K. Gupta, K.Y. Lee, A. Sohn, T.Y. Kim, K.S. Shin, D. Kim, S.K. Kim, K. H. Lee, H.J. Shin, D.W. Kim, S.W. Kim, Transparent flexible graphene triboelectric nanogenerators, *Adv. Mater.* 26 (2014) 3918–3925, <https://doi.org/10.1002/adma.201400172>.
- [8] D. Yoo, S. Lee, J.W. Lee, K. Lee, E.Y. Go, W. Hwang, I. Song, S.B. Cho, D.W. Kim, D. Choi, J.Y. Sim, D.S. Kim, Reliable DC voltage generation based on the enhanced performance triboelectric nanogenerator fabricated by nanoimprinting-poling process and an optimized high efficiency integrated circuit, *Nano Energy* 69 (2020), 104388, <https://doi.org/10.1016/j.nanoen.2019.104388>.
- [9] Z.-H. Lin, G. Cheng, S. Lee, K.C. Pradel, Z.L. Wang, Harvesting Water Drop Energy by a Sequential Contact-Electrification and Electrostatic-Induction Process, *Adv. Mater.* 26 (2014) 4690–4696, <https://doi.org/10.1002/adma.201400373>.
- [10] U. Khan, S.W. Kim, Triboelectric nanogenerators for blue energy harvesting, *ACS Nano* 10 (2016) 6429–6432, <https://doi.org/10.1021/acsnano.6b04213>.
- [11] J.H. Lee, S.M. Kim, T.Y. Kim, U. Khan, S.W. Kim, Water droplet-driven triboelectric nanogenerator with superhydrophobic surfaces, *Nano Energy* 58 (2019) 579–584, <https://doi.org/10.1016/j.nanoen.2019.01.078>.

- [12] D. Yoo, S.C. Park, S. Lee, J.Y. Sim, I. Song, D. Choi, H. Lim, D.S. Kim, Biomimetic anti-reflective triboelectric nanogenerator for concurrent harvesting of solar and raindrop energies, *Nano Energy* 57 (2019) 424–431, <https://doi.org/10.1016/j.nanoen.2018.12.035>.
- [13] S. Nie, H. Guo, Y. Lu, J. Zhuo, J. Mo, Z.L. Wang, Superhydrophobic cellulose paper-based triboelectric nanogenerator for water drop energy harvesting, *Adv. Mater. Technol.* 5 (2020) 1–9, <https://doi.org/10.1002/admt.202000454>.
- [14] S. Lin, L. Xu, A. Chi Wang, Z.L. Wang, Quantifying electron-transfer in liquid-solid contact electrification and the formation of electric double-layer, *Nat. Commun.* 11 (2020) 1–8, <https://doi.org/10.1038/s41467-019-14278-9>.
- [15] S. Saeidi, P. Zhang, T. Saboori, S. Wongwises, Z. Lin, J. Chen, A contextual framework development toward triboelectric nanogenerator commercialization, *Nano Energy* 101 (2022), 107572, <https://doi.org/10.1016/j.nanoen.2022.107572>.
- [16] H. Cho, J. Chung, G. Shin, J.Y. Sim, D.S. Kim, S. Lee, W. Hwang, Toward sustainable output generation of liquid-solid contact triboelectric nanogenerators: The role of hierarchical structures, *Nano Energy* 56 (2019) 56–64, <https://doi.org/10.1016/j.nanoen.2018.11.039>.
- [17] S. Lin, M. Zheng, J. Luo, Z.L. Wang, Effects of surface functional groups on electron transfer at liquid-solid interfacial contact electrification, *ACS Nano* 14 (2020) 10733–10741, <https://doi.org/10.1021/acsnano.0c06075>.
- [18] X. Li, L. Zhang, Y. Feng, X. Zhang, D. Wang, F. Zhou, Solid-liquid triboelectrification control and antistatic materials design based on interface wettability control, *Adv. Funct. Mater.* 29 (2019) 1–10, <https://doi.org/10.1002/adfm.201903587>.
- [19] S. Jang, M. La, S. Cho, Y. Yun, J.H. Choi, Y. Ra, S.J. Park, D. Choi, Monocharged electret based liquid-solid interacting triboelectric nanogenerator for its boosted electrical output performance, *Nano Energy* 70 (2020), 104541, <https://doi.org/10.1016/j.nanoen.2020.104541>.
- [20] S.S. Kwak, S. Lin, J.H. Lee, H. Ryu, T.Y. Kim, H. Zhong, H. Chen, S.W. Kim, Triboelectrification-Induced Large Electric Power Generation from a Single Moving Droplet on Graphene/Polytetrafluoroethylene, *ACS Nano* 10 (2016) 7297–7302, <https://doi.org/10.1021/acsnano.6b03032>.
- [21] W. Xu, H. Zheng, Y. Liu, X. Zhou, C. Zhang, Y. Song, X. Deng, M. Leung, Z. Yang, R. X. Xu, Z.L. Wang, X.C. Zeng, Z. Wang, A droplet-based electricity generator with high instantaneous power density, *Nature* 578 (2020) 392–396, <https://doi.org/10.1038/s41586-020-1985-6>.
- [22] G. Cheng, Z.H. Lin, Z.L. Du, Z.L. Wang, Simultaneously harvesting electrostatic and mechanical energies from flowing water by a hybridized triboelectric nanogenerator, *ACS Nano* 8 (2014) 1932–1939, <https://doi.org/10.1021/nm406565k>.
- [23] S. Hu, Z. Shi, R. Zheng, W. Ye, X. Gao, W. Zhao, G. Yang, Superhydrophobic Liquid-Solid Contact Triboelectric Nanogenerator as a Droplet Sensor for Biomedical Applications, *ACS Appl. Mater. Interfaces* 12 (2020) 40021–40030, <https://doi.org/10.1021/acsmami.0c10097>.
- [24] M. Xu, S. Wang, S.L. Zhang, W. Ding, P.T. Kien, C. Wang, Z. Li, X. Pan, Z.L. Wang, A highly-sensitive wave sensor based on liquid-solid interfacing triboelectric nanogenerator for smart marine equipment, *Nano Energy* 57 (2019) 574–580, <https://doi.org/10.1016/j.nanoen.2018.12.041>.
- [25] H. Zhang, Y. Yang, Y. Su, J. Chen, C. Hu, Z. Wu, Y. Liu, C. Ping Wong, Y. Bando, Z. L. Wang, Triboelectric nanogenerator as self-powered active sensors for detecting liquid/gaseous water/ethanol, *Nano Energy* 2 (2013) 693–701, <https://doi.org/10.1016/j.nanoen.2013.08.004>.
- [26] S. Lee, S.H. Bae, L. Lin, Y. Yang, C. Park, S.W. Kim, S.N. Cha, H. Kim, Y.J. Park, Z. L. Wang, Super-flexible nanogenerator for energy harvesting from gentle wind and as an active deformation sensor, *Adv. Funct. Mater.* 23 (2013) 2445–2449, <https://doi.org/10.1002/adfm.201202867>.
- [27] S. Jang, Y. Joung, H. Kim, S. Cho, Y. Ra, M. Kim, D. Ahn, Z.H. Lin, D. Choi, Charge transfer accelerating strategy for improving sensitivity of droplet based triboelectric sensors via heterogeneous wettability, *Nano Energy* 97 (2022), 107213, <https://doi.org/10.1016/j.nanoen.2022.107213>.
- [28] X. Li, L. Zhang, Y. Feng, Y. Zheng, Z. Wu, X. Zhang, N. Wang, D. Wang, F. Zhou, Reversible temperature-sensitive liquid-solid triboelectrification with polycaprolactone material for wetting monitoring and temperature sensing, *Adv. Funct. Mater.* 31 (2021) 1–11, <https://doi.org/10.1002/adfm.202010220>.
- [29] X. Yao, Y. Hu, A. Grinthal, T.S. Wong, L. Mahadevan, J. Aizenberg, Adaptive fluid-infused porous films with tunable transparency and wettability, *Nat. Mater.* 12 (2013) 529–534, <https://doi.org/10.1038/nmat3598>.
- [30] D. Tian, L. He, N. Zhang, X. Zheng, Y. Dou, X. Zhang, Z. Guo, L. Jiang, Electric field and gradient microstructure for cooperative driving of directional motion of underwater oil droplets, *Adv. Funct. Mater.* 26 (2016) 7986–7992, <https://doi.org/10.1002/adfm.201601843>.
- [31] Y. Huang, B.B. Stogin, N. Sun, J. Wang, S. Yang, T.S. Wong, A switchable cross-species liquid repellent surface, *Adv. Mater.* 29 (2017), <https://doi.org/10.1002/adma.201604641>.
- [32] K. Han, K. Yong, Overcoming limitations in surface geometry-driven bubble transport: bidirectional and unrestricted movement of an underwater gas bubble using a magnetocontrollable nonwetting surface, *Adv. Funct. Mater.* 2101970 (2021) 1–10, <https://doi.org/10.1002/adfm.202101970>.
- [33] G.Z. Li, G.G. Wang, D.M. Ye, X.W. Zhang, Z.Q. Lin, H.L. Zhou, F. Li, B.L. Wang, J. C. Han, High-Performance Transparent and Flexible Triboelectric Nanogenerators Based on PDMS-PTFE Composite Films, *Adv. Electron. Mater.* 5 (2019) 1–8, <https://doi.org/10.1002/aelm.201800846>.
- [34] Z. Chen, Y. Lu, R. Li, R.J. Orlando, R. Manica, Q. Liu, Liquid-solid triboelectric nanogenerators for a wide operation window based on slippery lubricant-infused surfaces (SLIPS), *Chem. Eng. J.* 439 (2022), <https://doi.org/10.1016/j.cej.2022.135688>.
- [35] S. Liu, X. Liu, G. Zhou, F. Qin, M. Jing, L. Li, W. Song, Z. Sun, A high-efficiency bioinspired photoelectric-electromechanical integrated nanogenerator, *Nat. Commun.* 11 (2020) 1–9, <https://doi.org/10.1038/s41467-020-19987-0>.
- [36] H.H. Singh, N. Khare, KPFM study of flexible ferroelectric polymer/water interface for understanding the working principle of liquid-solid triboelectric nanogenerator, *Adv. Mater. Interfaces* 2100032 (2021) 1–7, <https://doi.org/10.1002/admi.202100032>.
- [37] X. Dai, B.B. Stogin, S. Yang, T.S. Wong, Slippery wenzel state, *ACS Nano* 9 (2015) 9260–9267, <https://doi.org/10.1021/acsnano.5b04151>.
- [38] Y. Zeng, Y. Luo, Y. Lu, X. Cao, Self-powered rain droplet sensor based on a liquid-solid triboelectric nanogenerator, *Nano Energy* 98 (2022), 107316, <https://doi.org/10.1016/j.nanoen.2022.107316>.
- [39] L. Zhao, L. Liu, X. Yang, H. Hong, Q. Yang, J. Wang, Q. Tang, Cumulative charging behavior of water droplet driven freestanding triboelectric nanogenerators toward hydrodynamic energy harvesting, *J. Mater. Chem. A* 8 (2020) 7880–7888, <https://doi.org/10.1039/d0ta01698e>.
- [40] W. Yuan, C. Zhang, B. Zhang, X. Wei, O. Yang, Y. Liu, L. He, S. Cui, J. Wang, Z. L. Wang, Wearable, Breathable and Waterproof Triboelectric Nanogenerators for Harvesting Human Motion and Raindrop Energy, *Adv. Mater. Technol.* 7 (2022) 1–8, <https://doi.org/10.1002/admt.202101139>.
- [41] M. Xu, T. Zhao, C. Wang, S.L. Zhang, Z. Li, X. Pan, Z.L. Wang, High power density tower-like triboelectric nanogenerator for harvesting arbitrary directional water wave energy, *ACS Nano* 13 (2019) 1932–1939, <https://doi.org/10.1021/acsnano.8b08274>.
- [42] X. Wang, S. Fang, J. Tan, T. Hu, W. Chu, J. Yin, J. Zhou, W. Guo, Dynamics for droplet-based electricity generators, *Nano Energy* 80 (2021), 105558, <https://doi.org/10.1016/j.nanoen.2020.105558>.
- [43] D. Yoo, S.J. Kim, Y. Joung, S. Jang, D. Choi, D.S. Kim, Lotus leaf-inspired droplet-based electricity generator with low-adhesive superhydrophobicity for a wide operational droplet volume range and boosted electricity output, *Nano Energy* 99 (2022), 107361, <https://doi.org/10.1016/j.nanoen.2022.107361>.
- [44] N. Pereira, A.C. Lima, V. Correia, N. Perinha, S. Lanceros-Mendez, P. Martins, Magnetic proximity sensor based on magnetoelectric composites and printed coils, *Mater. (Basel)* 13 (2020) 1–8, <https://doi.org/10.3390/ma13071729>.
- [45] F. Wu, L. Marechal, A. Vibhute, S. Foong, G.S. Soh, K.L. Wood, A compact magnetic directional proximity sensor for spherical robots, *IEEE/ASME Int. Conf. Adv. Intell. Mechatronics, AIM*. 2016–Septe, 2016: 1258–1264. (<https://doi.org/10.1109/aim.2016.7576943>).
- [46] S. Paul, J. Chang, A. Rajan, S. Mukhopadhyay, Design of linear magnetic position sensor used in permanent magnet linear machine with consideration of manufacturing tolerances, *IEEE Sens. J.* 19 (2019) 5239–5248, <https://doi.org/10.1109/JSEN.2019.2903292>.
- [47] S. Hughes, A.J. El Haj, J. Dobson, B. Martinac, The influence of static magnetic fields on mechanosensitive ion channel activity in artificial liposomes, *Eur. Biophys. J.* 34 (2005) 461–468, <https://doi.org/10.1007/s00249-005-0484-x>.